First cryogenic test results of 3D-printed resonators for quantum bits

P R Carriere[1], P Frigola[1], R Agustsson[1], M H Chou[2], A N Cleland[2,3], T Horn[4], M Kelly[3], S V Kutsaev[1], R Povey[2] and A Y Smirnov[1]

[1]RadiaBeam Technologies LLC, Santa Monica, CA, 90404, USA
[2]Institute for Molecular Engineering, University of Chicago, Chicago, IL, 60637, USA
[3]Argonne National Laboratory, Lemont, IL, 60439, USA
[4] North Carolina State University, Raleigh, NC 27607, USA

E-mail: carriere@radiabeam.com

Abstract. Quantum computers (QC) have the potential to efficiently solve problems currently unfeasible on even the fastest generation of classical computers. The building block of a QC is a quantum bit (qubit). Encoding and reading qubit states coupled via high-Q resonant cavity modes is a solution to maintaining qubit states; however there is a need for simple, scalable and robust fabrication techniques capable of realizing high density cavity arrays. RadiaBeam is developing a novel approach utilizing metal additive manufacturing(AM) using both laser and electron beam powder bed fusion. Using a 6GHz quarter wave resonator (QWR), we fabricated several niobium and titanium alloy QWR cavities and characterized their superconducting RF performance. In this letter, we provide the details of the first 3D-printed qubit cavities design and fabrication, and compare their Q-factors, measured at dilution fridge temperatures, against the machined Nb resonators.

1. Introduction

The emerging field of quantum computing (QC) is rapidly growing and has shown immense potential. There is strong evidence that quantum computers possess a capacity exceeding the limits of classical computers and have the potential to efficiently solve problems currently unfeasible with current hardware, drastically advancing the frontiers of high energy physics and science in general [1]. The building block element of a QC is a quantum bit (qubit). Josephson junction circuits [2] are natural candidates for qubit blocks since they operate as non-linear quantum element. However, qubit state degrades rapidly due to the interaction with environmental degrees of freedom and the added control channels [3,4]. To avoid this problem, Josephson circuits can be protected from environmental noise and loss via the encoding qubits states in high-Q resonant cavity modes [5,6,7,8].

Superconducting niobium cavities used in particle accelerators are able to reach quality factors of ~10^{10}, potentially enabling storage times approaching seconds, even at the single-photon level [9]. Traditionally, accelerator superconducting radio frequency (SRF) cavities are fabricated by forming, electron beam welding, chemically etching and heat treating ultra-high purity niobium sheet[^{10}]. Generally, this approach is focused on sub-3.9 GHz components, as the frequency dependent BCS surface resistance is comparable to the residual resistance when operating in the superfluid helium bath. However, due to the noise considerations and dilution fridge space limitations, future quantum information science (QIS) systems will likely operate in the frequency range of 6 GHz to 15 GHz and at millikelvin temperatures, enabling a new class of superconducting materials with transition temperatures below 2K. Furthermore, QIS will consist of many individual cavity qubit units coupled


Content from this work may be used under the terms of the Creative Commons Attribution 3.0 licence. Any further distribution of this work must maintain attribution to the author(s) and the title of the work, journal citation and DOI.
Published under licence by IOP Publishing Ltd

together. For these applications, the development of a simple, inexpensive and robust fabrication methods is desired.

In response to this problem, we have successfully fabricated QWRs using two different metal additive manufacturing (AM, a.k.a. 3D-printing) technologies; electron beam powder bed fusion (EB-PBF), and laser powder bed fusion (L-PBF) (See Figure 1).

Figure 1: (Left) Array of niobium QWRs printed using EB-PBF on a titanium build plate; (Center) Ti-6Al-4V (Ti64) L-PBF QWR fitted with SMA coupling ports; (Right) Ti64 SLM QWR undergoing room temperature RF testing.

AM of passive microwave components is of growing interest due the rapid and efficient fabrication of complex geometries. Additive manufacturing of superconducting cavities has been previously demonstrate in titanium (Ti-6V-4Al) and aluminium (Al-12Si), achieving quality factors of $3x10^4$, $4x10^6$ respectively[11,12]. Additively manufactured superconducting niobium resonators have demonstrated quality factors varying from $2x10^5$ to $1x10^9$, with the latter requiring post-print machining [13,14].

Building on these results, we have demonstrated superconducting QWRs using two related AM technologies: EB-PBF and L-PBF. In both powder bed fusion (PBF) processes, the build platform is lowered, fresh powder is recoated over the build platform and the melting process is repeat from 2D slices into a 3D part. In this case, the distinguishing feature between PBF processes is electron beam (EB-PBF) versus laser PBF pencil beam.

Compared to L-PBF, EB-PBF offers a series of unique capabilities including a high vacuum build environment for reduced residual gas contamination, direct beam heating of the part for reduced residual stress and high (6 kW) average beam power. Conversely, L-PBF yields better geometric accuracy and surface finish due to the finer powder, smaller layers thicknesses and smaller spot sizes. Since L-PBF is performed in pressurized inert gas atmosphere, oxygen pickup from powder to printed part can be significantly higher than EB-PBF.

2. Design

Broadly speaking, the Q-factor of the resonator can be defined according to $Q = G/R_s$, where G[Ω] is the cavity geometry factor and Rs[Ω] is the RF surface resistance. In order to maximize the cavity quality factor, and thus the qubit coherence time, it is imperative that the resonator has a high G-factor via shape optimization, as well as low surface resistance, via material selection, fabrication and post-processing. Recently, we have developed a superconducting 3D quarter-wave resonator (QWR) machined from accelerator-grade niobium [15]. This 6 GHz cavity was designed for a G=71Ω, which was chosen as a compromise between machinability and RF performance. For comparison, superconducting elliptical cavities used for accelerators operating in the TM_{010} mode have a corresponding G≈268 Ω, while QWR have a reported G as high as 110Ω [16]. The corresponding 3D cavity design as well as the corresponding electric and magnetic field distributions simulated in COMSOL, are shown in Figure 2.

To compare the performance of the AM QWRs with the machined ones, we replicated their nominal RF design in the printed parts. While useful for comparison, this approach does not fully leverage the advantages of additive manufacturing in terms of component integration or shape optimization. The layer-wise nature of the process results in anisotropy in both the material properties as well as the surface

finish. Surface finish is another key difference in as-built AM parts, with the best surface finish achieved on upward facing surfaces and the worst finish associated with downward facing surfaces.

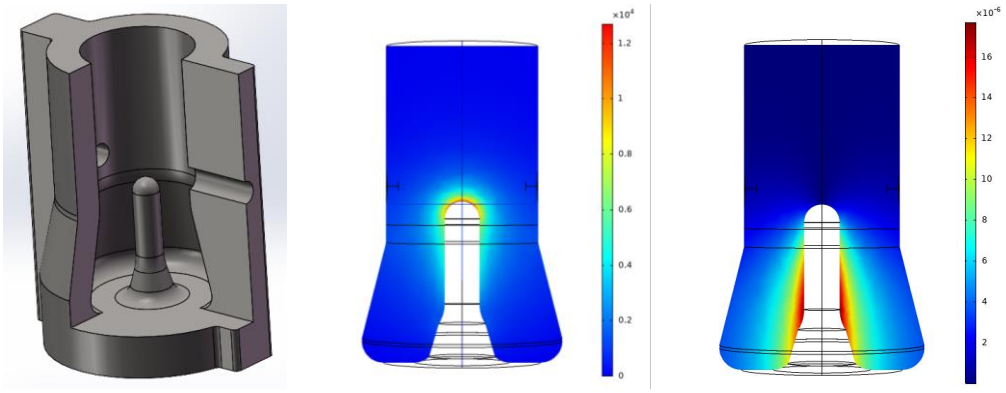

Figure 2 (Right) Sectioned CAD model of QWR, with total part height of 28mm. (Center) Electric field distribution simulated in COMSOL (Right) Magnetic field distribution

3. Fabrication

Within the broader field of additive manufacturing (AM), each material/process pair has achieved a certain technological maturity. We opted to print identical QWR designs from grade 5 titanium (Ti-6wt% Al – 4wt% V), ie Ti64, using the L-PBF process, which is a mature turn-key technology offered from numerous of service bureaus. The transition temperature of Ti64 ranges between T_c = 1.3-6.3K with the variation due to oxidation treatment and annealing state [11]. We also printed QWRs from pure niobium (T_c = 9.26K) using the EB-PBF process, which is relatively undeveloped technology well suited for printing refractory metals such as niobium. Comparison of materials and processes was performed as a first attempt to understand which technology is best suited for further technological development.

Our Ti64 QWR geometries were commercially printed using a Concept laser M2 printer (Castheon Inc, Thousand Oaks, CA). Virgin 15-45μm plasma atomized powder was used with print parameters tuned to reduce the surface roughness of the inner RF surfaces. After printing, the parts were hot isostatically pressed (HIP) using established procedures adapted from aerospace applications (KittyHawk Inc, Garden Grove, CA). The HIP process homogenizes the microstructure, eliminates print-related residual stress and reduces process-induced internal porosity. One Ti64 QWR was sent to a commercial vendor for proprietary Chemical-Mechanical Polishing (REM Surface Engineering, Southington, CT). Approximately 200μm of material was removed from the part, resulting in a surface roughness reduction from Ra = 9.7 to 0.9μm, as measured on the upper bore of the cavity. Both Ti64 cavities underwent a final, 30s etch in Krolls etchant [9% vol HF(48% conc.) 12% vol HNO3(70% conc.), remainder water], resulting in a mass loss of approximately 0.17g. While this number corresponds to a thickness reduction of about 11μm, some powder particles were visually observed in the rinse water, suggesting an overestimation of material removal.

As mentioned, EB-PBF of niobium is a relatively new AM process and was performed in collaboration with North Carolina State University using a custom Arcam S12 printer [17]. The niobium powder was plasma atomized from ASTM B392 type 1, reactor-grade wire. Limited contamination from wire to powder was measured except for an increase of light interstitial elements(C, O, N, H), a feature consistent with the high surface area associated with powder. The Nb powder was sieved to -100/+230 mesh in an inert glove box, yielding a D_{10} = 55μm and D_{90} = 127μm. Some titanium powder cross contamination was observed within the Nb feedstock, likely due to inadequate cleaning of the sieving station.

The Nb parts were printed at a sustained temperature of approximately 1300°C, as measured using a two-color pyrometer focused on the top of build surface. Both Nb cavities were manually polished with an alumina slurry and etched in a buffered chemical etchant [25% vol HF(48%.) 25% vol HNO3(70%.), remainder H3PO4 (95% conc.)] for 120 seconds, with a mass loss of 0.75g and an estimated material removal of 12μm.

Both cavities underwent a small amount of external machining, including milling flat surfaces for contact with the SMA probes and reaming coupling ports for the electric coupling antennas.

4. Resonator Characterization

The accessible surfaces of the QWR's RF surfaces were microscopically inspected for geometric accuracy and surface finish. Images of the centrepin top hemispheres are shown below, comparing the surfaces of various materials and finishing techniques.

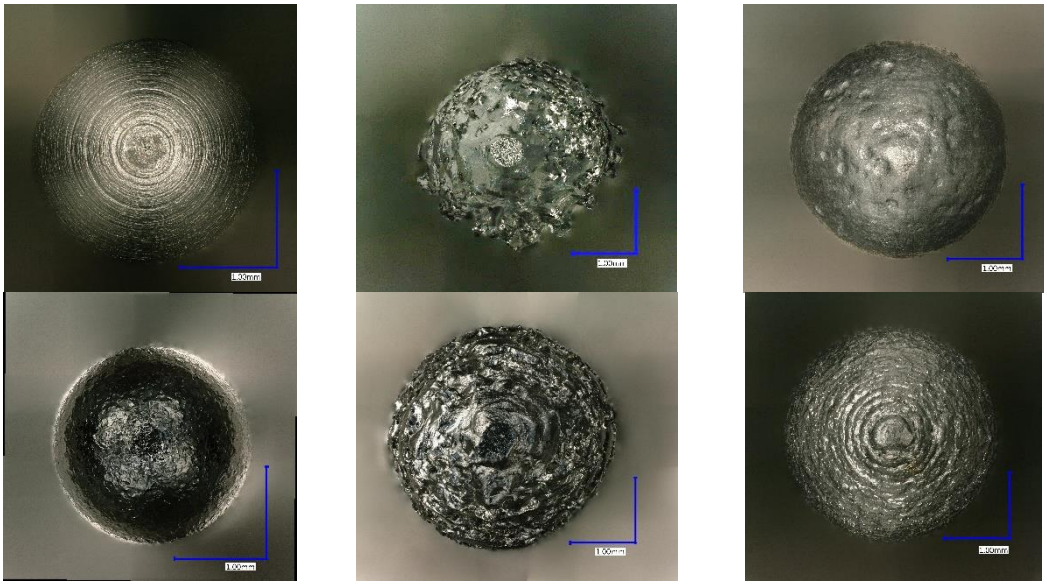

Figure 3 Optical microscope images of the 6 GHz QWR center pin. (Left upper) As-machined Nb cavity (Left lower) Machined and etched Nb cavity (Center upper) EB-PBF 3D printed niobium *Cavity 1* (Center lower) EB-PBF Nb *Cavity 2* (Right upper) L-PBF 3D printed Ti64 *Cavity 3* with heavy material removal via abrasive finishing (Right lower) L-PBF 3D printed Ti64 *Cavity 4*

The accelerator grade machined and etched niobium center pins, shown in the first column of Figure 3, exhibit clear machining marks and grain definition in the etched part. Also shown are the centrepins of two niobium EB-PBF printed parts, as wells as the equivalent parts printed in Ti64 using the L-PBF process. From these images, we immediately note that the surface finish of the laser-printed Ti64 parts is superior to the electron beam equivalent, a direct result of smaller spot size and powder size. We also note that the abrasively finished Ti64 *Cavity 3* has a macroscopically smoother finish that the as-printed equivalent, as the finishing process effectively removes adhered powder particles. The differences in niobium *Cavity 1* and *Cavity 2* surface finish is due to the differences in abrasive polishing times applied to the parts, with *Cavity 1* having longer material removal times.

Table 1: Room temperature RF measurements

			Q-factor		
#	Material	Fabrication Method	Expected	Measured	f_0[MHz]
	Copper	Machined	3492	3312	6027.7
	Niobium	Machined, Etched (-89μm)	1190	1069	6045.5
1	Niobium	EB-PBF, abrasive polish and etched (-10um)	1190	425	5991.8
2	Niobium	EB-PBF, abrasive polish and etched (-10um)	1190	487	6113.2
3	Ti64	L-PBF, HIP, tumbled, etched (-10um)	622	345	5962.6
4	Ti64	L-PBF, HIP, etched (-10um)	622	296	5894.4

4.1 Q-factor measurements

Prior to cryogenic testing, the room temperature Q-factors of the cavities were measured, with a summary comparing machined Nb and Cu cavities against the performance of the AM Ti64 and Nb cavities, Table 1.

The room temperature electrical conductivity of each cavity was measured using a 480kHz eddy current probe (Fischer Technology SigmaScope SMP10). From the center frequency and conductivity measurements, we calculate the equivalent room temperature RF surface resistance value (R_s) and assuming that G= 71Ω, estimate the idealized, smooth surface Q factor. While the resonant frequency data shows that the overall cavity shape is accurately rendered by the AM processes, printing and post-processing requires significant improvement.

Following room temperature RF measurements, the cavities were assembled in a magnetically shielded and thermally engineered RF test stand, then fastened to the base of a dilution fridge (Blue Fors BF-LD400) at the University of Chicago. RF tests were performed at a mixing chamber temperature of 20mK, as measured with a calibrated RuO_2 sensor. These tests did not have on-cavity thermometry, therefore precise determination of the superconducting transition temperature was not possible. Subsequent tests with instrumented cavities showed a temperature differential between the mixing chamber and the cavity on the order of 40mK while at base temperature. A schematic of the 4-cavity RF test assembly, as well as an image of the assembly fastened to the dilution fridge, is shown in Figure 4 below.

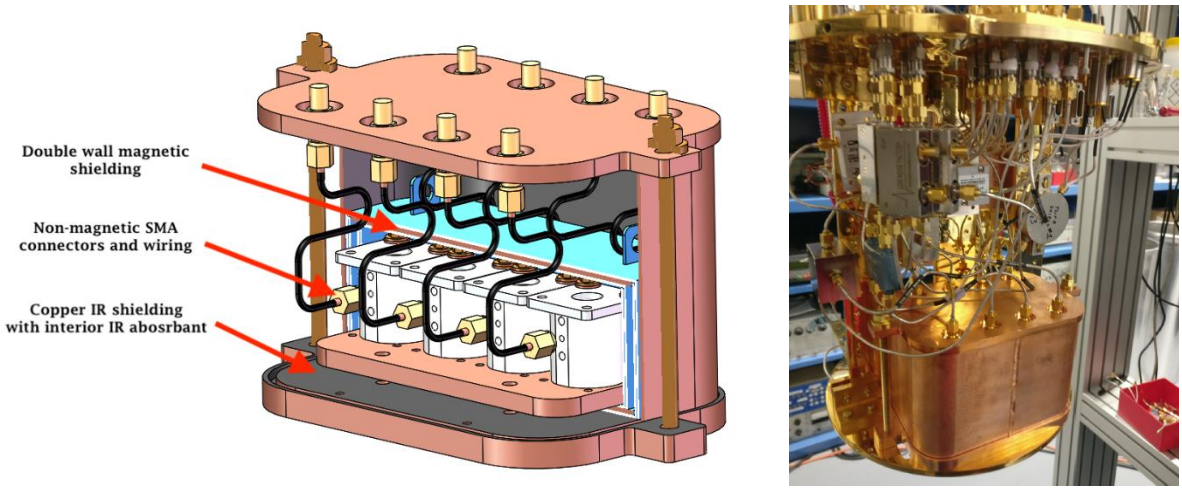

Figure 4 (Left) CAD model of 4-cavity dilution fridge RF test fixture; (Right) Fixture installed on the University of Chicago's dilution refrigerator.

The cryogenic measurements were performed using an RF amplification chain detailed elsewhere[15], which includes -20dB attenuation at 4K and -6dB attenuation at mixing chamber. The complete [S] parameter measurements for all cavities was performed using a vector network analyser with an output power range of -20 to -90dBm. We extracted the loaded quality factors as well as the coupling quality factors under the assumption of equal splitting, as the multiplexed measurement does not allow self-deterministic extraction of the coupling factors [18]. The corresponding resonance frequency, as well as the calculated unloaded quality factor, are summarized in Table 2.

Table 2: Dilution fridge superconducting RF measurements

			Q_0	f_0[MHz]
	Niobium	Machined, Etched (-89μm)	9.2×10^6	6192.9
1	Niobium	EB-PBF, abrasive polish and etched (-10um)	1.6×10^6	6008.7
2	Niobium	EB-PBF, abrasive polish and etched (-10um)	1.2×10^6	6130.4

3	Ti64	L-PBF, HIP, tumbled, etched (-10um)	0.4×10^6	5980.5
4	Ti64	L-PBF, HIP, etched (-10um)	2.2×10^6	5917.1

In addition to the network analyser measurements, we also performed time-domain ring-down measurements, whereby the cavity is excited at resonance, the drive signal is turned off and the ring-down decay curve is capture on an oscilloscope, providing the loaded Q factor. Our measurements showed good agreement between both time domain and frequency domain measurements. Also, we did not observe meaningful loaded quality factor power dependence over the range of measurements.

5. Analysis

The quality factor of a resonant cavity represents a global measurement of the cavity losses, weighted by the field distribution at specific surfaces. High field regions, such as the center pin, will have an outsize effect on the performance of the cavity, with multiple RF loss channels contributing in parallel. This concept extends to the intrinsic surface anisotropy associated with additive manufacturing, with upward facing surfaces having the best finish and downward facing surfaces the worst. Post-processing is crucial to normalizing the finish and reducing the surface resistance of the entire 3D geometry.

Besides the G factor, normal conducting quality factors are dependent on the conductivity of the bulk material, as well as roughness-enhanced losses. In the case of the precision machined copper and niobium QWRs, we see that measured Q is within 95% and 90% of the calcualted value, respectively. Compared to the RF skin depth, the machined surfaces are smooth with minimal surface area enhancement. Furthermore, the center frequencies are measured to within 1% of the design frequency (6000MHz), with deviations attributable to machining tolerances and etching anisotropy.

The larger center frequency spread of the AM cavities is attributable to the geometric accuracy of the printing process as well as the variability of the surface finishing. In terms of Q, the Nb AM cavities are 35% and 40% of the idealized value. Similarly, the abrasively finished Ti64 AM cavity had an Q of 55% of ideal, while the etched cavity was 47%. Although the absolute Q of the Nb AM cavities is higher than the Ti AM cavities, the comparative value of Nb relative to ideal is lower. This result is to be expected considering the Nb QWR were printed using the EB-PBF process, which is based on coarser powder, thicker layers and larger beam diameters.

In addition to surface roughness, superconducting resonators are sensitive other loss channels, including magnetic flux trapping, two-level losses, contamination, hydride formation, etc. While it is difficult to assign an absolute magnitude to each of these losses without more detailed measurements, the AM Nb cavities had a Q of roughly 15% of the machined part, with the degradation likely a function of both reduced material purity increased surface roughness. Furthermore, the etched Ti64 *Cavity 4* had a higher Q than both AM-Nb cavities. This inversion is surprising, considering the lower superconducting transition temperature of Ti64. Furthermore, it is surprising to note that the Ti64 *Cavity 3*, which underwent heavy abrasive finishing, had the worst performance of all. Our current hypothesis is that these increased losses are attributed to lossy ceramic media embedded in the RF surface. Further destructive analysis of the cavity is required to confirm this result.

While normal conducting measurements provide a rapid method for characterizing the surface finish and geometric accuracy of the printed parts, our results demonstrate that these results cannot be translated to superconducting performance. In fact, the best room temperature AM cavity had the worst superconducting properties; demonstrating that material, printing and post-processing have to all be considered for optimization.

6. Conclusions and future plans

This report represents preliminary RF measurements of additively manufactured quarter wave resonators at millikelvin tempertures. Although both Nb and Ti64 QWRS exhibited Q-factors significantly lower than conventionally machined parts, these initial results are encouraging and suggest the need for further process development. Specifically, AM-specific RF designs, high vacuum heat treatment and electropolishing are all currently under development. Additional thermometry and surface analysis is planned for the future.

These initial results highlight the opportunity for fabricating unmachinable RF geometries with additive manufacturing. For quantum information systems and detectors, seamless arrays of densely packed 3D cavities with customized resonances can be rapidly designed, printed and tested, with minimal engineering and manufacturing effort. Overall, 3D-printing of superconductors has immense potential for future research, and may produce new applications which will be of great benefit in physics and engineering.

7. References

[1] R Raz, A. *Electronic Colloquium on Computational Complexity*, Report No. 107 (2018)
[2] B. D. Josephson, *Phys. Lett.* 1 **(7):** 251–253, 1962
[3] H. Dieter Zeh, *Foundation of Physics*, **vol.** 1, pp. 69-76, (1970).
[4] A Chailloux, *Intl Conf on the and Appl of Cryptology and Information Security*. Springer, Cham, 2017.
[5] P. J. Leek *et al*.,, *Phys Rev Let* **104.10**, 100504 (2010), 0911.4951
[6] M. A. Sillanpaa *et al*., *Nature* **449**, 438–442, 2007.
[7] J. Gambetta *et al*., *Phys. Rev. A* **74**, 042318, 2006
[8] A.A. Houck *et al*., *Phys. Rev. Lett.* **101**, 080502, 2008.
[9] S. Kuhr *et al*., *Appl. Phys. Lett*. **90**, 164101 (2007).
[10] H Padamsee, *RF superconductivity: science, technology, and applications (2009)*. Wiley
[11] E Holland, *et al*., *Appl. Phys. Lett* **111.20**, 2017
[12] D Creedon *et al*., *Appl. Phys. Lett* **109.3** (2016)
[13] B McAllister *et al*., *IEEE Trans on Inst and Meas* **70** (2020): 1-7.
[14] P Frigola *et al Proceedings of SRF2015*, THPB042, Whistler, Canada
[15] S Kutsaev *et al., EPJ Quantum Tech*, **7:7**, 2020.
[16] J Sharping *et al*. *Jour App Phys* **128.7** (2020): 073906.
[17] C Ledford, *et al. Applied Sciences* **9.19** (2019): 3993.
[18] M Anthony, *et al. Applied Physics Letters* 100.11 (2012): 113510.

Acknowledgements
This work was supported by the U.S. Department of Energy, Office of High Energy Physics, under SBIR grants DE- SC0018753 and DE-SC0019973. The authors would like to thank Dr. Zachary Conway (BNL), Mr. Thomas Reid (ANL), Dr. Alexander Romanenko and Dr. Timergali Khabibouline (FNAL) for their valuable advice.